Mechanics of Cellulose Nanocrystals and their Polymer Composites

Anahita Pakzad and Reza S. Yassar

Abstract The fabrication of cellulose nanocomposites with ultimate mechanical properties has received tremendous attention during the past decade. However, the published data has not been reviewed and systematically compared from mechanical point of view. The current study aims to fill this gap by providing a critical review on the published data on the mechanics of cellulose nanocrystals and their composites. The studies on individual cellulose nanocrystals show that their strength depends on the number and type of inter and intra hydrogen bonds on the cellulose chains, which are affected by the cellulose type and origin. It has been shown that the tensile modulus, yield strength and creep resistance are higher in cellulose nanocomposites than in unfilled polymers. However, above optimum cellulose content, the agglomeration of nanocrystals degrades the mechanical properties. Furthermore, cellulose nanocrystals enhance the structural stiffness of polymer composites at elevated temperatures. Formation of rigid nanocrystal network causes increase in the storage modulus (E′) and glass transition temperature.

1 Introduction

Nanocomposites have attracted great attention in the scientific community because of the significant enhancement in the base materials by the addition of nanofillers.

A. Pakzad and R. S. Yassar (✉)
Mechanical Engineering-Engineering Mechanics, Michigan Technological University, 1400 Townsend Drive, Houghton, MI 49931, USA
e-mail: reza@mtu.edu

A. Pakzad
e-mail: apakzad@mtu.edu

Adv Struct Mater (2013) 4: 233–263
DOI: 10.1007/8611_2010_38

Published Online: 16 November 2010

Extensive publications exist on the mechanical properties [26, 41, 78], thermal stability [42, 81], superconductivity [59], and electrical magnetic behavior [14, 71] of various nanocomposites. A wide variety of synthetic nanofillers have been used to reinforce polymer matrices, for instance see [37, 44, 56, 64].

Because of the current environmental issues such as global warming and environmental pollution, investigations are being shifted toward the use of natural fillers in nanocomposites [11, 57, 72]. Since natural nanocomposites are infinitely recycled in the nature, use of these fillers decreases carbon dioxide release, and consequently the final product will be more environmental friendly. Cellulose nanocrystal is a natural polymer, which for the first time was used by Favier et al. [23] to reinforce polymers.

Cellulose exists in the structure of plants (Fig. 1), sea animals and it is also made by some bacteria and it mostly functions as the reinforcing structure. It is being considered as one of the most abundant materials in the nature and has many other qualities that make it attractive for usage in fabrication of composite materials. A number of these exceptional qualities are: renewable nature, biodegradability, biocompatibility, lower cost in comparison to synthetic fillers, low density, impressive strength to weight capability, easy processability because of its nonabrasive nature and relatively reactive surface [4, 5, 13, 27, 33, 54, 58, 61].

The chemical structure of cellulose is shown in Fig. 2. It is a linear homopolymer of β-D-glucopyranose units which are connected by (1 → 4)-glycosidic bonds. Cellulose is chiral and because of high density of hydroxyl groups is hydrophilic and can be soluble in water depending on n (n differs from 500 to 15,000). Cellulose is easily machinable and is degradable by enzymes.

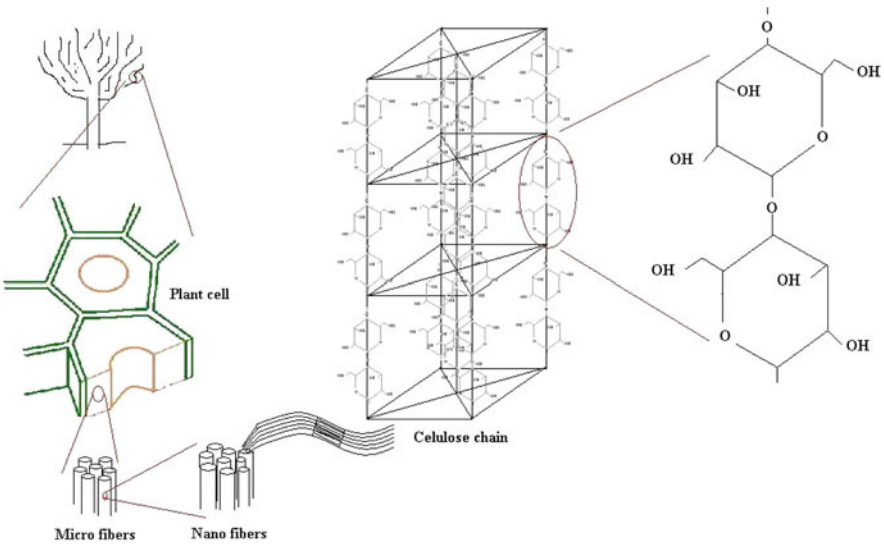

Fig. 1 From plant stem to cellulose (not in scale). Cellulose crystals are the building bricks of plant cells

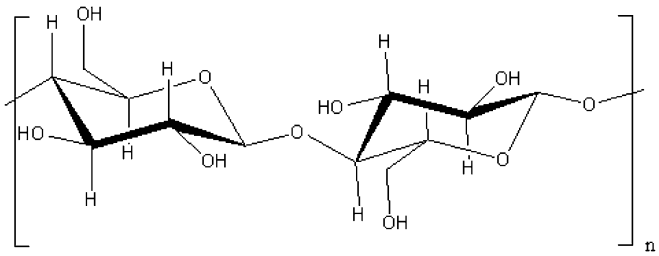

Fig. 2 Chemical structure of cellulose

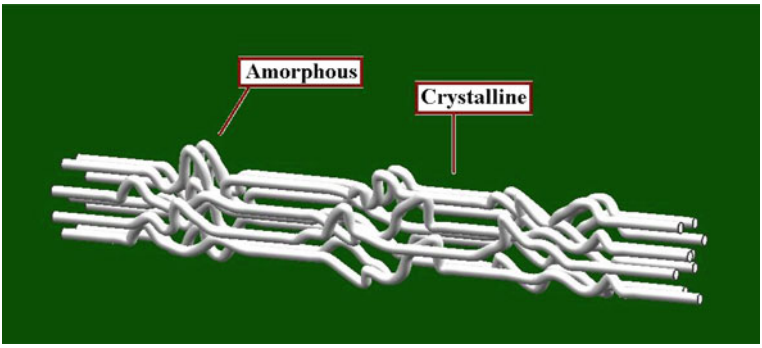

Fig. 3 Schematic presentation of crystalline structure of cellulose I, crystalline parts are connected by amorphous areas

The straight nature of cellulose molecule and the existence of hydrogen bonds result in high likeliness of crystallization. Pure cellulose exists in different allomorphs [33, 85]. Cellulose I (natural or native cellulose), which is semi crystalline, contains two phases, crystalline triclinic I_α and amorphous monoclinic I_β. Amorphous areas connect the crystalline parts as shown in Fig. 3. The proportion of these two phases depends on the origin of the cellulose. For instance, I_α is more found in bacteria and algae, while I_β is more found in plants.

Cellulose II (regenerated or man-made) is a recrystallized form of cellulose I, and in contrast to cellulose I, has anti parallel strands and inter-sheet cellulose bonding, and it is thermodynamically more stable. Cellulose III can be formed by treating cellulose with liquid ammonia. Depending on what the starting material, cellulose I or II, the ammonia treatment conversion will be denoted as III_1 or III_2 respectively. Cellulose III is amorphous. Heat treatment of cellulose III results in cellulose IV, which is also amorphous.

A wide variety of sources has been investigated for preparation of cellulose crystals. The main four groups are wood [10], agricultural byproducts (cotton [10], wheat straw [18]), animal cellulose (sea tunicate [2, 73]) and bacteria [10, 29]. For more references see [39].

The most common method for separation of cellulose crystals from amorphous region is acid hydrolysis (Fig. 4). This includes a chemical treatment for separation of nanocrystals and use of mechanical energy to disperse them in an aqueous suspension. Under suitable conditions (e.g. see [7]), acid hydrolysis breaks down the structure of cellulose into individual needle like crystalline rods by disrupting the amorphous regions. This separation happens due to the faster hydrolysis kinematics of amorphous regions than the crystalline parts. The resultant highly crystalline cellulose nanostructures with different aspect ratios (L/D, L = length, D = diameter), that depend on the hydrolysis conditions and their crystallinity and origin and can be >200 [10, 22, 66], are referred to as *cellulose nanocrystals* (CNXLs). One should note that CNXLs have been entitled, nanorods, nanowires and whiskers [39]. All these terms refer to the individual crystalline rods of cellulose which have at least one dimension less than 100 nm and an overall length comparable to their diameter. Figure 4 shows a scanning electron microscopy (SEM) image of starting material, microcrystalline cellulose (MCC), and a transmission electron microscopy (TEM) image of the final product of acid hydrolysis, CNXLs.

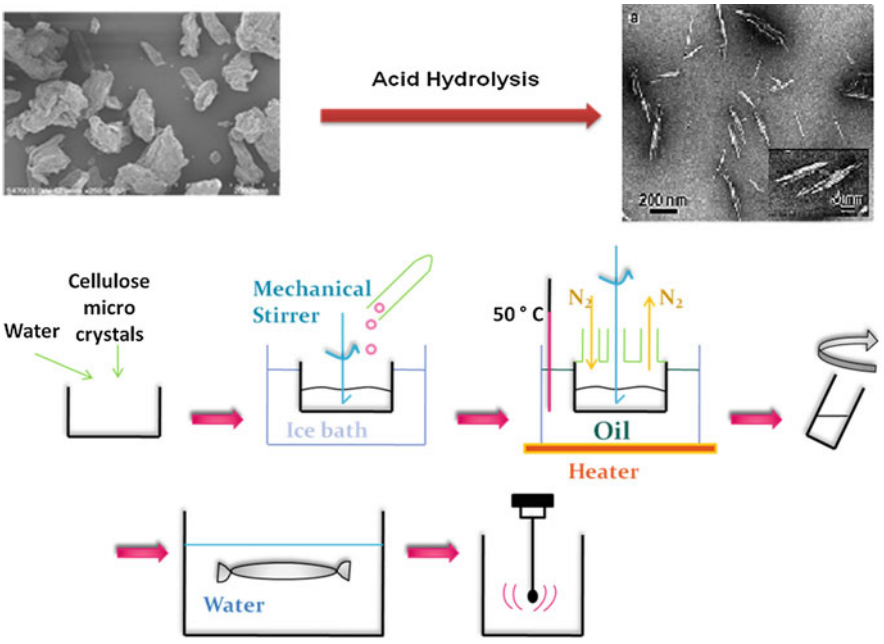

Fig. 4 Schematic procedure of acid hydrolysis of commercially available microcrystalline cellulose. After the acid (e.g. H_2SO_4) is added slowly to the water solution, it should be heated to a certain temperature and kept for a specific time. Afterwards using centrifuge, dialysis against distilled water, sonication and maybe ultra filtering CNXLs are separated (TEM sample: Elazzouzi et al. [22]

2 Mechanics of CNXLs

The mechanical properties of cellulose-based structures have been investigated from both modeling and experimental prospective. Early modeling works started in 1930 but were limited to cellulose in general and not nanocrystals in particular. Meyer and Lotmar [55] were the first who theoretically modeled the mechanical properties of cellulose. They showed that its elastic modulus corresponded to the chain direction of the cellulose crystal and could be calculated from the force constants of the chemical bonds of the chain gained from vibrational frequencies of the molecules. Their modeling was later modified and extended to crystals of synthetic polymers, nylon and Terylene by Lyons [51]. Treloar [77] further modified these models by considering the relation of valence angle deformation to the forces applied to the chain.

Theoretical work on mechanics of nanocrystals has received attention only very recently. Tanaka and Iwata [74] used molecular mechanics simulation and derived values between 124 and 155 GPa for elastic modulus of natural nanocellulose fibers. For this characterization the super cell models with crystal sizes of $1 \times 1 \times 10$ and $4 \times 4 \times 10$ were used (Fig. 5), which in comparison to the unit cell method did not require strict symmetries and thus were more suitable for polymers. In order to calculate the elastic modulus, linear relation between the changes in energy density and the half of the square of the compressive or tensile strain was used:

$$\frac{p - p_0}{S * l} = \frac{1}{2} E \left(\frac{l - l_0}{l_0} \right)^2 \tag{1}$$

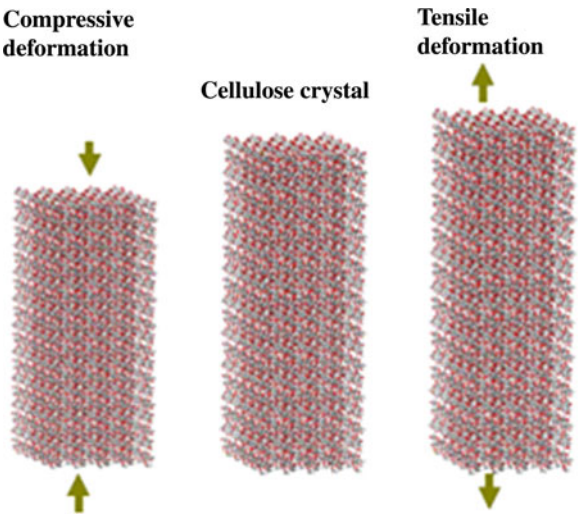

Fig. 5 Molecular mechanics simulation representing compressive and tensile deformation of the CNXLs. The *arrows* show the direction of the applied stresses [74]

where P and P_0 are the potential energy of the cellulose crystal under stress and non-stress energy conditions respectively; S is the cross section, l_0 is the length of the crystal under non-stressed condition, and l is the length of the crystal. The authors reported that the elastic modulus calculated in $4 \times 4 \times 10$ unit-cell size had smaller deviations (124–172 GPa) and were closer to the observed values (138 GPa [60]) in comparison to the values calculated in $1 \times 1 \times 10$ unit-cell size (89–173 GPa).

Experimental measurement of mechanical properties of cellulose began in 1962 but the work was not focused on nanocrystalline cellulose at that time. Sakurada et al. [69] studied the crystal deformation of highly oriented fibers of cellulose I (native cellulose) by X-ray diffraction. For this purpose a Geiger counter X-ray diffractometer was used, a constant stress σ was applied to the fiber bundle, and the fractional change in the length of two glucose units $\Delta I/I_0$, or of a net plane distance, $\Delta d/d_0$, was calculated from the displacement of the interference maximum (Eq. 2):

$$\varepsilon = \Delta I/I_0 = \Delta d/d_0 \tag{2}$$

Finally the elastic modulus, E, was calculated by $E = \sigma/\varepsilon = 137$ GPa (Fig. 6). Mann and Roldan-Gonzalez [53] also used X-ray diffraction and measured elastic moduli between 70 and 90 GPa for crystals of cellulose I and cellulose II, respectively.

The same procedure was recently used by Nishino et al. [60] to measure the elastic modulus of different polymorphs of cellulose. The results are summarized in Table 1. The value obtained for cellulose I is in accordance with what Sakurada et al. [69] obtained many years before.

Atomic force microscopy (AFM) is another tool that has been used for measuring the elastic modulus of cellulose fibers [15, 30, 40]. In this method the AFM tip is used to deflect a nano sized cellulose fiber, which is suspending on a groove. In the work performed by Guhados et al. [30] sonicated suspension of bacterial cellulose fibers was placed on a silicon grating with step height of 1,000 nm and a

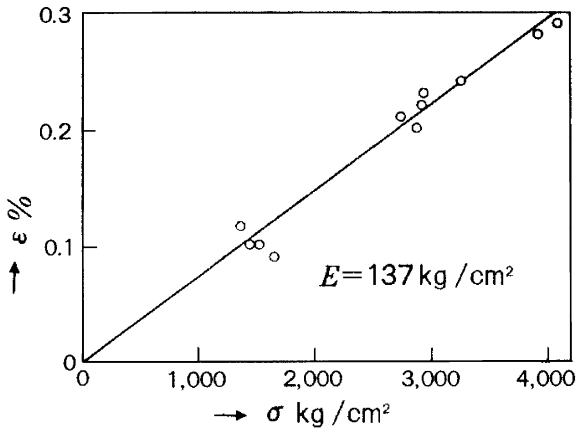

Fig. 6 Stress-strain for highly oriented fibers of cellulose I obtained by X-ray measurements. The elastic modulus was calculated from the slope to be 137 GPa [69]

Table 1 Elastic modulus of crystalline regions of cellulose polymorphs obtained by X-ray diffraction [60]

CNXL origin	Elastic modulus (GPa)
I	138
III_I	87
IV_I	75
II	88
III_{II}	58

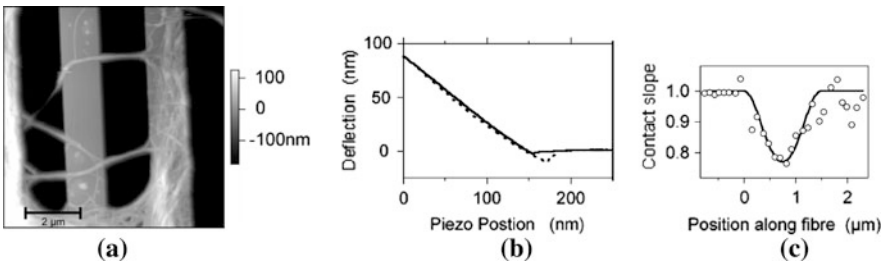

Fig. 7 **a** AFM image of bacterial cellulose fibers suspended over a gap, **b** force spectra obtained near the middle of a suspended fiber (*solid* approach, *dashed* retraction). **c** Slope of force spectra along a suspended 1.62 µm fiber. The suspended parts have smaller slope than the supported ones [30]

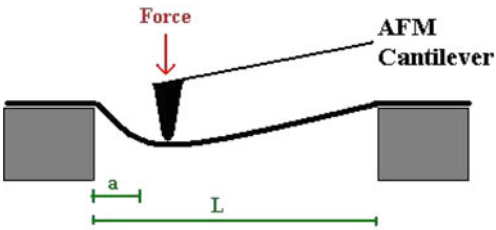

Fig. 8 Clamped fiber with length equal to (L). Force is applied to the fiber with distance (a) from the edge using the AFM cantilever tip [30]

pitch of 3 µm and then it was spin coated. Fibers with diameters <100 nm were identified by AFM imaging and then using force-volume mode, force spectra were gained for an array of positions along the fibers (Fig. 7).

It was assumed that the fibers had elliptical cross sections and that they were clamped on both ends. The slope of the force spectra, *dy/dz*, that was measured along the fibers was then calculated to be:

$$\frac{dy}{dz} = \left[1 + \frac{k}{3EI}\left(\frac{a(L-a)}{L}\right)^3\right]^{-1} \tag{3}$$

where k is the spring constant of the AFM cantilever, I is the area moment of inertia, L is the length of the fiber, a is the position of loading with respect to one end (Fig. 8), and E is the elastic modulus of the fiber which is unknown.

The elastic modulus was calculated 78 ± 17 GPa, which was consistent with Voigt model [34].

Cheng and Wang [15] used AFM and measured the elastic modulus of cellulose fibers isolated from Lyocell fibers in a three-point bending test to be 93 GPa. Recently, Iwamoto et al. [40] used AFM to perform three point bending tests on CNXLs obtained by sulfuric acid hydrolysis of tunicate and obtained a value of 150.7 GPa. AFM seems to be a useful tool for characterization of the mechanical properties of single CNXLs (Table 2). These measurements rely on good knowledge of the geometry of the sample, which is obtained from AFM imaging, and can be affected by tip broadening parameter.

Raman spectroscopy is another well established technique which has been used for measurement of the elastic modulus specifically the elastic modulus of CNXLs. These measurements are based on the shift in the characteristic Raman band (located at 1,095 cm^{-1}) that corresponds to the vibration of C–O–C bonds on the back bone of the CNXLs (Fig. 9). To conduct these measurements, CNXLs are usually embedded in epoxy, and a macro-scale bending test is performed.

In 2005, Sturcova et al. [73] measured the elastic modulus of tunicate CNXLs to be around 143 GPa using this technique. In this case the position of the Raman band peak was linearly dependent on strain up to the value of about 0.8% (Fig. 10). Formations of a plateau after 0.8% strain was related to the weakening of the cellulose-matrix interface and as a result decrease in the stress transfer efficiency.

Table 2 Elastic modulus of CNXLs with different origins, gained using atomic force microscopy

CNXL origin	Elastic modulus (GPa)	Reference
Bacterial	78	[30]
Lyocell fibers	93	[15]
Tunicate	150.7	[40]

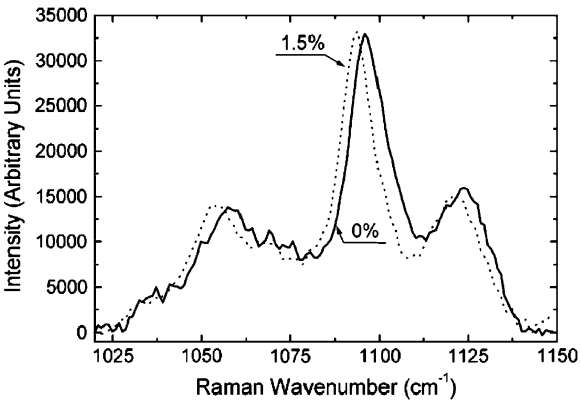

Fig. 9 Typical Raman band shift of the 1,095 cm^{-1} peak of tunicate cellulose subjected to tensile strain [73]

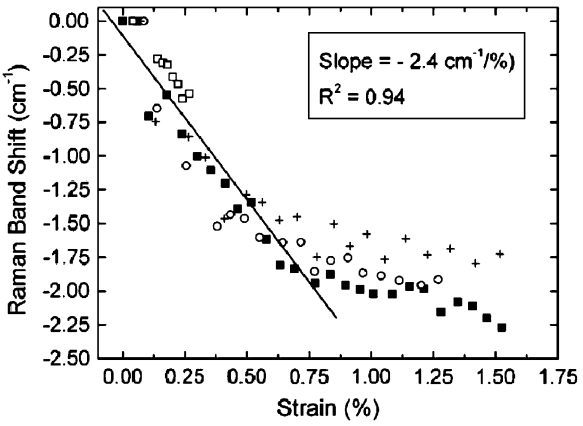

Fig. 10 The Raman band shift in the 1,095 cm^{-1} as a function of strain for tunicate cellulose [73]

Table 3 Elastic modulus of CNXLs with different origins, gained using Raman spectroscopy

CNXL origin	Elastic modulus (GPa)	Reference
Tunicate	143	[73]
Cotton	105	[68]
Bacterial	114	[38]

$$E = \frac{d\sigma}{d(\Delta v)} \times \frac{d(\Delta v)}{d \in} \tag{4}$$

$$\mathrm{E}_c = \eta_0 \mathrm{E}_\mathrm{f} \tag{5}$$

By substituting $d(\Delta v)/d \in = 2.4$ $cm^{-1}\%$ (from Fig. 10) and value of $d\sigma/d(\Delta v) = 4.7$ cm^{-1}/GPa [20, 21], in Eq. 4, the elastic modulus of two dimensional network tunicate cellulose was calculated to be 51.1 GPa. Eq. 5 was then used to obtain the elastic modulus of a single fiber of CNXL (E_f). In this equation E_c is the elastic modulus of a two dimensional random network of fibers and η_0 is the efficiency factor equal to $9/8\pi$.

The drawback for this modeling approach is that Eqs. 4 and 5 are based on the assumption of well compacted fibers. Moreover the fact that cellulose was embedded in matrix, the nature of chemical bonding between cellulose and matrix and the distribution of CNXLs can play a role in the calculated elastic modulus.

Recently, the same technique was used to measure the elastic modulus of cotton CNXLs and bacterial CNXLs (Table 3). Hsieh et al. [38] obtained the value of 114 GPa for the elastic modulus of bacterial CNXLs and Rusli and Eichhorn [68] found an upper value of 105 GPa and a lower value of 57 GPa for the elastic modulus of cotton CNXLs. Both of the values for cotton CNXLs are lower than the value for tunicate cellulose measured by Sturcova et al. [73] and the value for bacterial cellulose reported by Hsieh et al. [38]. This may be due to the smaller aspect ratio in cotton-based cellulose than the aspect ratio of other CNXLs which might have resulted in less effective stress transfer.

One could ask what causes such high elastic modulus in a low density polymer such as cellulose. To answer this question, we should go back to the molecular structure of cellulose (Fig. 11). There are multiple hydroxyl groups on the cellulose chain. These can make intermolecular and intramolecular hydrogen bonds which have a key role in the mechanics of this material. When a cellulose chain goes under tension, hydrogen bonds bear the load and deform. This continues until the load reaches the strength of these bonds, and these break (yield point). After this point, C–O–C bridges come into the picture and take the majority of the load [43, 45].

Number and nature of the hydrogen bonds greatly affect the mechanical properties of cellulose nanocrystals. For example, Tashiro and Kobayashi [75] showed that the intramolecular hydrogen bonds in cellulose II fibers are weaker than those in cellulose I, but their intermolecular bonds are the same. This results in higher elastic modulus for cellulose I than II.

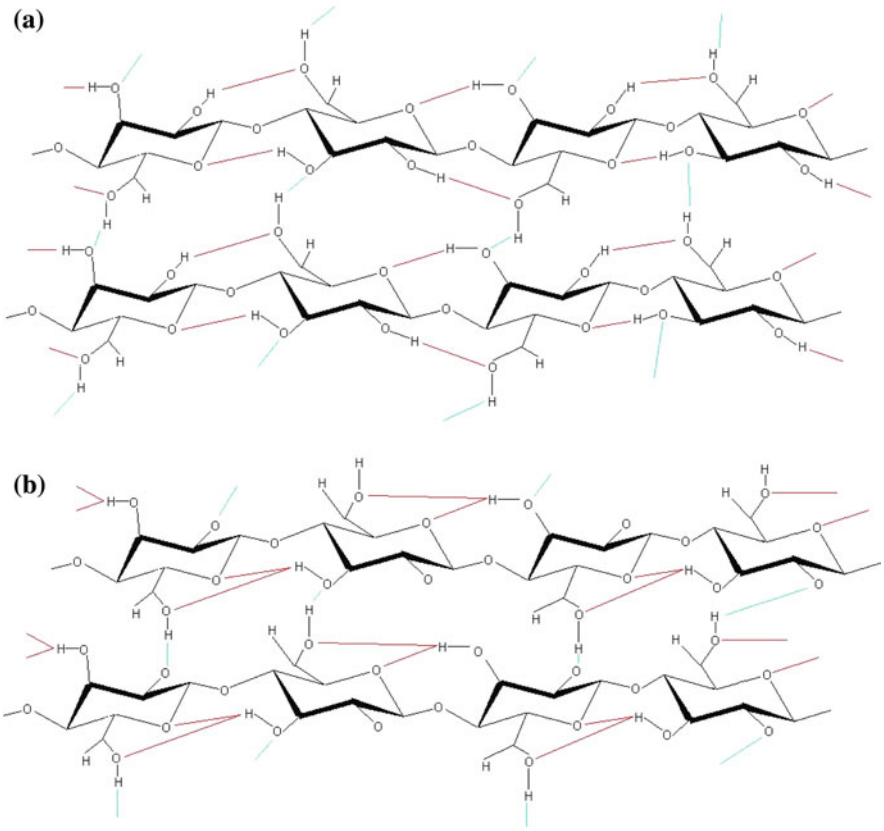

Fig. 11 Intermolecular (*blue*) and intramolecular (*red*) hydrogen bonds in cellulose I (**a**) and cellulose II (**b**)

Table 4 compares the elastic modulus and tensile strength of CNXLs with carbon nanotubes, steel and glass fiber. As it can be seen mechanical properties of CNXLs are much higher than those of glass fiber and stainless steel and are slightly lower than carbon nanotubes. This makes them promising candidates for reinforcement phase of composites materials specifically because unlike carbon nanotubes they are definitely biocompatible and biodegradable.

3 Mechanics of CNXL Composites

In a composite system reinforcements are used to carry the mechanical loads, improve the properties and lower the cost of the final product. On the other hand, matrix, which in our case is a polymer, is there to increase the toughness, to disperse fillers and to transfer the load to the fillers. Nanofillers are used widely these years because they have less defects and higher surface area compared to larger sized fillers. Thus nanofillers bring additional improvements and unique characteristics to the final product, at lower filler content levels as compared to micro and macro fillers.

Like all composite materials, the properties of cellulose nanocomposites depend on the properties, the volume fraction, and the spatial arrangement of the matrix and the reinforcement. Dispersion of CNXLs in the polymer matrix is not an easy procedure, and evenly distributed reinforcement is crucial for enhancement of the mechanical properties of composites. This can be specially challenging in the cases that polymer matrix is hydrophobic (as opposed to hydrophilic CNXLs). Without changing the surface activity and dispersion qualities of CNXLs (described later) the ultimate mechanical properties of the nanocomposite may not be much different or they may even be less compared to the pure polymer.

On the other hand, the main factors that dictate their mechanical properties are:

The aspect ratio of the CNXLs (L/D): This ratio depends on the origin of the crystals and the higher it is the better the mechanical properties will be [46, 52, 63].

CNXLs from different origins will have diverse size distributions, surface properties and more importantly different aspect ratios. All of these have fundamental influence on the mechanical properties of the final composition. Figure 12 shows differences in the elastic modulus of composites made of starch (with elastic modulus <2 GPa) and 5 wt% CNXL from various origins.

Table 4 Strength and stiffness of CNXLs compared to other materials

Material	Tensile strength (GPa)	Elastic modulus (GPa)
Cellulose crystal	7.5–10 [33]	143 [73]
Glass fiber [17]	3	72
Steel [17]	0.9	215
Carbon nanotubes [83]	11–63	270–950

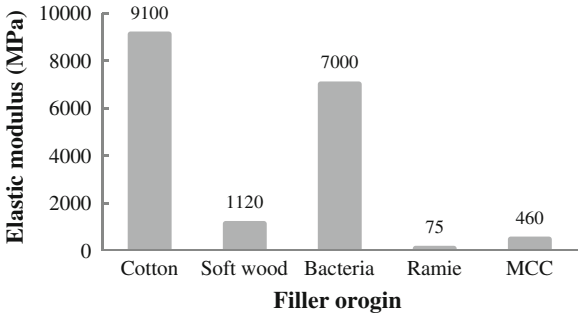

Fig. 12 Effect of CNXL origin on the Young's modulus of CNXL/starch composites [46, 52, 63]

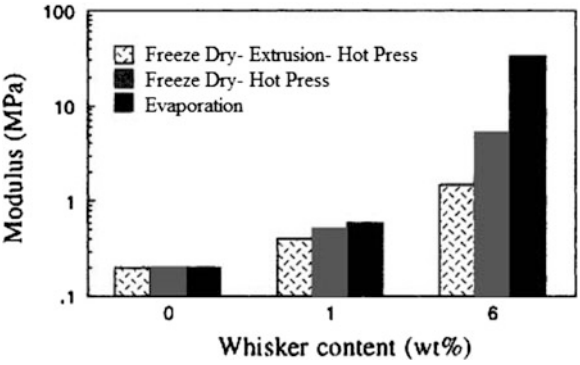

Fig. 13 Effect of processing method on the Young's modulus of CNXL/latex composites [32]

The processing method: Extrusion, hot pressing and evaporation are some techniques that are used. These techniques affect the orientation of the filler, the filler/filler interactions and may cause breakage of the fillers (changing the aspect ratio). They ultimately affect the final mechanical properties of the nanocomposite (Fig. 13). For instance, in the case of CNXL/latex composites, it has been shown that the efficiency of the processing methods is: extrusion < hot-pressing < evaporation [32].

The resulting competition of matrix/filler and filler/filler interactions: The preferred condition in most of composite materials is the matrix/filler, as opposed to the case in cellulose nanocomposites. Here the filler/filler interactions should be predominant, so that a 3D network of CNXLs is made to keep the week polymer in place and yield in higher stiffness and thermal stability in the resulting material [4, 24]. Percolating threshold, above which this 3D network is formed, is the critical volume fraction (v_{RC}), which separates the local and infinite communication of the fillers. It depends on the particle interactions and orientation and aspect ratio of fillers and it can be calculated using Eq. 6 [4]. Based on this equation, percolating threshold for composites with high aspect ratio fillers can be as low as 1%.

$$v_{RC} = \frac{0.7}{L/d} \tag{6}$$

Although filler/filler interactions need to be predominant, in order for the stress to be effectively transferred to the filler, good adhesion between the filler and matrix is vital [36, 28, 29], and not all polymers will have good adhesion with CNXLs. In order to optimize the interfacial bonding of the filler and the matrix, some modifications are possible. These include physical methods (e.g. changes in the structure and surface of CNXLs by coating them with surfactant [36]) and chemical modifications (e.g. grafting them with hydrophobes [25, 29]). One drawback to these procedures is that modified CNXLs have less reinforcing effects than not modified ones. This is due to the destruction of 3D network of CNXLs, as a result of changes in hydrogen bondings during these modifications. Another possibility can be the less efficient stress transfer from the polymer to CNXLs [28, 29].

Isotactic polypropylene (iPP), which is a hydrophobic polymer can be discussed as an example of surface modified cellulose crystals. Ljungberg et al. [50] prepared the iPP nanocomposites with aggregated CNXLs (CNXL-A), aggregated CNXL grafted with maleated polypropylene (CNXL-G-P), and surfactant-modified CNXL (CNXL-S), and compared their mechanical properties. At large deformations, where the mechanical properties depend chiefly on the dispersion quality of the fillers, failure to disperse CNXL-A homogenously, resulted in inferior mechanical properties than pure iPP. On the other hand, incorporating CNXL-G-P and CNXL-S into iPP enhanced the mechanical properties at large deformations as well as in linear ranges. This was due to the fact that their modified surface made good distributions and stress transfer possible (Fig. 14).

Following is a review on the studies that have been performed to characterize the tensile, nanoindentation, creep and thermo mechanical properties of CNXL-based nanocomposites.

3.1 Tensile Properties

Tensile tests are usually performed in universal test machines on pure polymer matrix and nanocomposite samples which are molded or cut in dog bone or

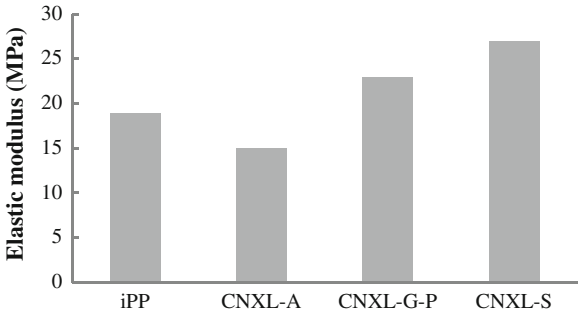

Fig. 14 Effect of CNXL surface modification on the Young's modulus iPP composites with 6 wt% tunicin CNXL [50]

rectangular shapes. Important mechanical properties such as elastic modulus, tensile strength, yield strength and ductility, can be derived from the load–displacement or stress–strain curves. Furthermore, by studying the shape of these curves one can gain useful information about the morphology of the ultimate nanocomposite and the dispersion quality if the reinforcements. For instance no necking can be a representative of well dispersion of filler in the polymer.

Compared to non-reinforced polymers, CNXL-based composites show improvements in tensile modulus and yield strength [3, 4, 13, 16, 46, 48, 54, 61, 65, 67, 82]. Figure 15 depicts the changes in mechanical properties of two different polymers (soy protein isolate (SPI) and polyvinyl alcohol (PVA)) before and after addition of CNXLs derived from cotton linters. Although the total trend is that the tensile strength and elastic modulus increase by adding CNXLs to polymers, the amount and quality of these strongly depend on the polymer and its interaction with CNXLs.

In general, an optimum filler content is desired in order to achieve the ultimate mechanical properties [16, 67, 79]. After this optimum value, the addition of filler content may result in the reduction of tensile strength and/or elastic modulus due to phase separation which occurs because of agglomeration of the nanofillers (see the strength data on Fig. 15). This optimum filler content depends on the characteristics of the polymer matrix and its interaction with nanocrystals. The tensile strength and/or elastic modulus decrease with addition of more cellulose and this is due to phase separation which occurs because of agglomeration of the nanofillers.

Elongation at break mostly decreases with addition of CNXLs, meaning that the material is modified from being ductile (with long deformation after yield until fracture) to very brittle (with almost no plastic deformation after yielding point; Fig. 15). Addition of a hard filler to a soft matrix results in higher strength at the cost of ductility. The reduction in elongation at break is a sign of good filler/filler and filler/matrix interactions, which restricts the motion of the polymer matrix.

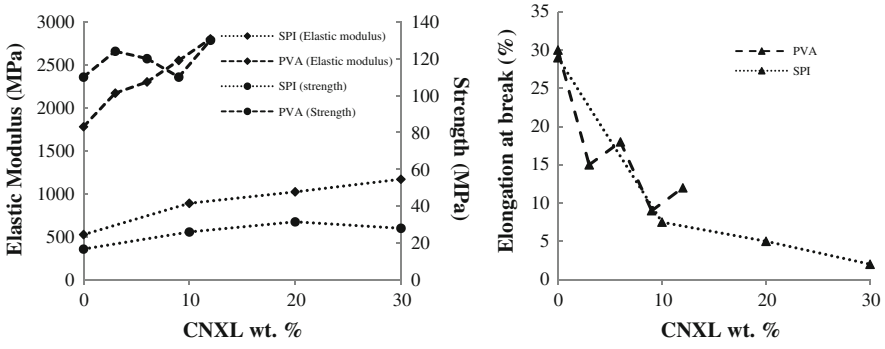

Fig. 15 Change in elastic modulus and tensile strength (*left*) and elongation at break (*right*) of soy protein isolate (SPI) and polyvinyl alcohol (PVA) filled with different amounts of CNXL derived from cotton linter [67, 79]

Table 5 summarizes the mechanical properties of various CNXL-polymer composites. Although this table does not cover all the published literature, it can be a good reference for comparison of the effect of cellulose origins and polymer types on the ultimate mechanical properties of these nanocomposites and the optimum filler content.

Experimental conditions such as temperature and relative humidity have great effects on tensile test results. For example as it is seen in Fig. 16, increase in the relative humidity (RH), tends to degrade the mechanical properties of cellulose nanocomposites with hydrophilic matrices [19, 79]. This is because at high humidity levels, hydrophilic polymer absorbs large amounts of water. As a result the matrix/filler interactions declines and CNXLs become surrounded by a week and soft phase, and the reinforcing effect of CNXLs diminishes.

3.2 Nanoindentation Studies

Another technique for mechanical characterization of polymer composites is nanoindentation. Nanoindentation is similar to macro-hardness tests but is done in nano-scales. Typically a diamond indentation tip with known elastic modulus and hardness is pressed into the surface of the sample, and the applied normal load (P) and the indentation height into the surface (h) are measured continuously during the loading and unloading. A schematic load–displacement curve is shown in Fig. 17. The elastic modulus (E) and hardness (H) are then calculated using the slope of the unloading part of the curve (S) and the equations below:

$$S = \frac{dP}{dh} = \frac{2}{\sqrt{\pi}} \boldsymbol{E}_r \sqrt{A} \tag{7}$$

$$\frac{1}{E_r} = \frac{(1 - v^2)}{E} + \frac{\left(1 - v_i^2\right)}{E_i} \tag{8}$$

$$H = \frac{P_{\max}}{A} \tag{9}$$

S is the slope of the load–displacement curve, which is obtained by fitting a second order polynomial function to the curve and differentiation (dP/dh). A is the projected contact area. As opposed to conventional indentation techniques, here the contact area is measured indirectly using the indentation height and the known geometry of the indenter. E_{r} is the reduced elastic modulus (the measured elastic modulus includes effects from both the specimen and the indenter), v_i, v and E_{i}, E are the Poisson's ratios and the elastic moduli of the indenter and the sample respectively [62].

Although several nanoindentation experiments have been reported for cellulose nanofiber reinforced polymer composites, no reports were found on nanoindentation results on CNXL composites. In this section two examples of nanoindentation

Table 5 Mechanical properties of various CNXL-polymer composites

Polymer				CNXL		Optimum composite				Reference
Name	Elastic modulus (MPa)	Strength (MPa)	Elongation at break (%)	Origin	Content variation	Filler content (%)	Elastic modulus (MPa)	Strength (MPa)	Elongation at break (%)	
Polyvinyl acetate	1,780	110	30	Cotton linter	0–12	12	2,800	130	12	Roohani et al. [67]
Soy protein isolate	526.4	16.73	29	Cotton linter	0–30	30	1,170	28	2	Wang et al. [80]
Waterborne polyurethane	0.5	4.3	1,086	Flax fiber	0–30	30	334.4	14.9	186	Cao et al. [13]
Polyurethane	41.16	14.05	0.55	Cellulose micro crystal	0–5	5	100.28	8.74	0.26	Marcovich et al. [54]
Modified potato starch	370	11.3	25	Cellulose micro crystal	0 and 5.3	5.3	460	13.7	32	Kvien et al. [46]
Plasticized wheat starch	55.9	2.8	94.2	Ramie	0–40	40	479.8	6.9	13.6	Lu et al. [52]
Unsaturated polyether	0.81	0.4	82	Tunicin	0–6	6	22.3	10.6	62	Azizi Samir et al. [6]

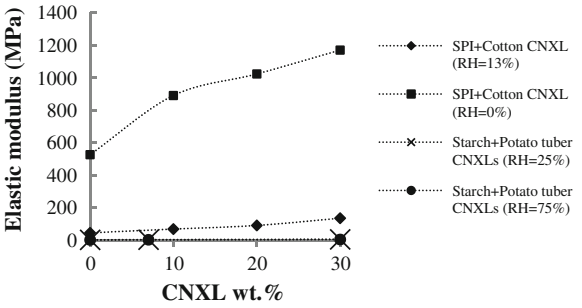

Fig. 16 Change in elastic modulus of soy protein isolate (SPI) and Starch filled with CNXL at various relative humidity (RH) [19, 79]

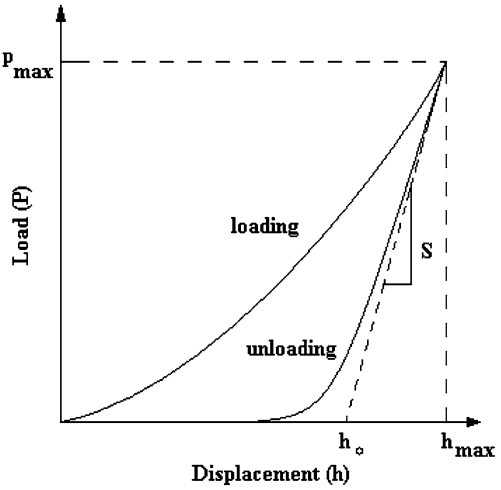

Fig. 17 Typical load–displacement curve [62]

results are discussed. Polymers in this section are all reinforced with cellulose nanofibers, which as opposed to CNXL that consist of only crystalline parts, have some amorphous regions too.

Zimmermann et al. [84] compared the elastic modulus of hydroxypropyl filled with cellulose nanofibers gained from two different methods of tensile and nanoindentation tests. The elastic modulus of the filled polymer was higher than the unfilled one in both methods, but nanoindentation resulted in higher values in comparison to tensile tests (Fig. 18). This dissimilarity may have different reasons. Firstly the elastic modulus of polymers depends on the available free volume, in nanoindentation this volume is less than in tension tests. Secondly, the volume of the sample on which the test is performed is bigger in tensile testing than in nanoindentation, this bigger volume contains larger amount of deflections such as microscopic cracks. And thirdly, the strain rates in these two methods are different and it is well known that the elastic modulus can be highly affected by the strain rate in many materials.

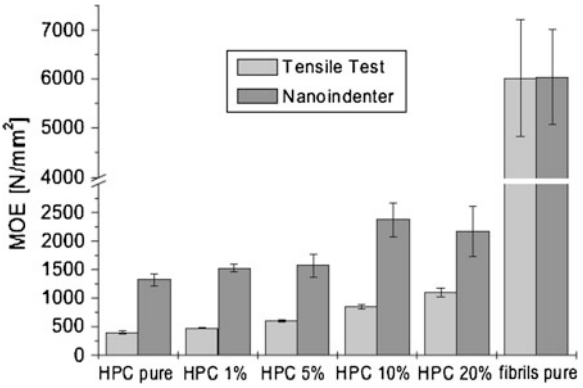

Fig. 18 Comparison the elastic modulus (MOE) values gained from tensile and nanoindentation tests on hydroxypropyl-cellulose nanofiber composites. Although the values gained for MOE from nanoindentation tests are higher than those gained from tensile tests, in both methods MOE increases as the amount of cellulose nanofiber is incresed in the nanocomposite [84]

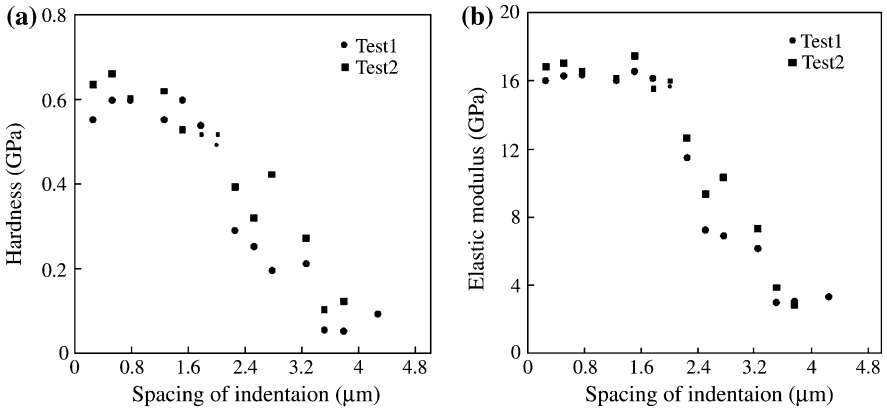

Fig. 19 Change in **a** hardness and **b** elastic modulus across the interphase region obtained by nanoindentation with 30 nm depth and 260 nm spacing [49]

As it was mentioned before, the stress transfer quality between filler and matrix is of significant importance in the mechanical studies of nanocomposites. The area that bonds cellulose nanofibers to polymer matrix is called *interface*. At the interface the properties change from the properties of individual nanofibers to the one in polymer matrix. The interface has crucial effects on the stress transfer qualities and has been motivation of great deal of studies and investigations. Lee et al. [49] evaluated the interface properties of polypropylene (PP) filled with cellulose nanofibers, using nanoindentation and compared the results with finite element analysis (FEA). A series of indentation tests with different indentation depth and different spacing were performed on the samples. According to the nanoindentation results with 30 nm depths and 260 nm spacing (Fig. 19), it was concluded that the width of the interface region was less than one micron. FEA results showed that the perfect interface width would be approximately 1.8 μm. Therefore, it was concluded that using the conventional techniques it would be

difficult to calculate the true mechanical properties of the interface in an area at least 8 times smaller than the indent size. At areas smaller than this value, the effect of neighboring materials becomes dominant which potentially can affect the experimental results.

Care should be taken during analysis of nanoindentation results for polymer composites. There are some debates that the famous Oliver-Pharr method [62], should not be used for polymer materials [76]. One should be careful when comparing results from nanoindentation tests on different materials, using different tips, techniques and in different laboratories. There are some phenomenon which can affect the test results. For example: Pile up is bulding out of the free surface of the material, which changes the contact area, and ultimately the E and H calculations. Viscoelasticity characteristics of polymers affects the unloading curves, and results in what is called a "nose" on the curves, where the indentation height increases while the load is being decreased. This results in negative values for contact stiffness (S). Finally the morphology of the indentation surface is vastly affected by sample preparation techniques that can result in different microstructures with different mechanical properties and/or various microscopic roughnesses. These ultimately give various E and H for various positions on one specific sample and increase the standard deviations from the average values.

3.3 Creep Properties

A limited number of investigations have been conducted on creep properties of CNXL composite systems. It is expected that due to stiffer nature of cellulose than the polymer matrix, CNXLs restrict the motion and reorientation of the polymer chains. This can influence the stress transfer and results in the enhancement of creep resistance in nanocomposite material [3]. Figure 20 shows that the addition of even a small amount of CNXL (0.1 to 1%) to polyurethane considerably decreases the creep strain.

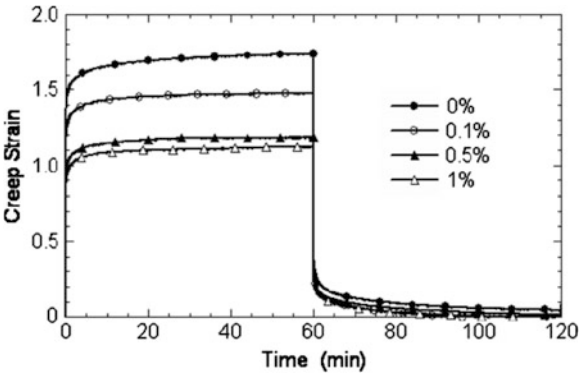

Fig. 20 Creep *curves* for unfilled polyurethane and CNXL/polyurethane nanocomposites with different wt. % (tests conducted at 20°C for 60 min). Due to the restricted motion of polymer chain by CNXLs, the creep resistance increases by increasing the filler even to a very small amount [3]

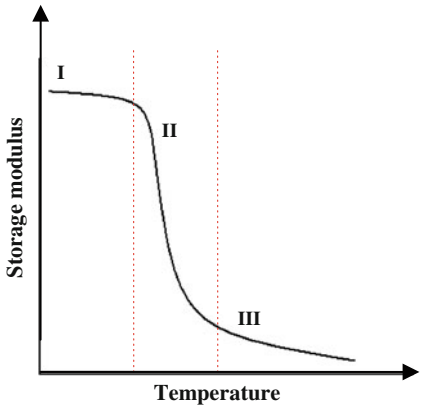

Fig. 21 Temperature dependence of storage modulus in a Thermoplastic polymer *I* glassy *II* glass transition *III* viscous liquid

3.4 Thermo-Mechanical Characterization

Thermo-mechanical characteristics of CNXL composites are mostly investigated using dynamic mechanical analysis (DMA), where the storage modulus (tensile: E' or shear: G') and the position of tan δ peak (the loss factor, $\tan\delta = \frac{E''}{E'}$ where $E''$is the loss modulus) are compared in the pure polymer and in composites with different filler contents. DMA is mostly performed in tensile (E') or sheer (G') mode, in a wide range of temperatures around the glass transition temperature of the polymer. These tests are usually done with a constant frequency (e.g. 1 Hz) and they provide information about the visco-elastic properties of materials.

Figure 21 shows a schematic curve of changes in storage modulus by temperature for a thermoplastic. This curve contains three phases:

(1) At temperatures below T_g or glassy stage, the storage modulus remains almost constant with increase in temperature.
(2) As the temperature approaches T_g, a dramatic drop in the storage modulus is observed where the material is being transformed from glassy to rubber state.
(3) Above T_g, polymer turns into a viscous liquid, and storage modulus keeps decreasing with increase in temperature.

Generally cellulose nanocomposites have been found to be more thermally stable than the matrix alone. Again, enough CNXL content causes a continuous 3D network (percolation), which reduces the mobility of polymer matrix and as a result the storage modulus (E' or G') increases and tan δ peak broadens. Above melting temperature (T_m) is where CNXLs have the most effect on thermo mechanical properties of the composites. As opposed to pure polymer, here storage modulus does not drop by increase in temperature, thus performance at high temperatures is improved and thermal stability is brought to the ultimate material up to degradation temperature of cellulose (around 500 K). Another thermo mechanical observation in nanocomposite polymers filled with CNXL is increase in glass transition temperature (T_g). This phenomenon is related to change in the

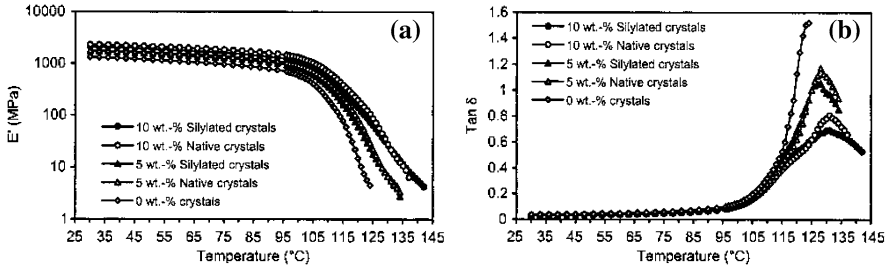

Fig. 22 Temperature dependence of storage modulus (**a**) and tan δ peak (**b**) in CNXL composites. Nanocomposites of native CNXL are thermally more stable than unfilled cellulose acetate butyrate and nanocomposites of silylated CNXL [29]

kinetics of the glass transition due to the presence of the nanocrystals and also increase in cross linking and as a result decrease in the mobility of the polymer chains. Broad amount of work has been concentrated on the thermo mechanical properties of CNXL polymer composites, for instance see: [1, 3, 5, 6, 8, 12, 13, 16, 23, 29, 31, 35, 46, 50, 52, 54, 65, 67, 79, 80].

Figure 22 depicts the results obtained from DMA tests on nanocomposites of cellulose and cellulose acetate butyrate [29]. Adding 10 wt. % native cellulose resulted in 94% improvement, at 81°C, and 2,000% improvement, at 124°C, in E′. Tan δ peak is also shown to go to higher temperatures and lower magnitudes and to broaden as the amount of filler was increased.

4 Morphological Analysis

For information on polymer microscopy readers can see Sawyer and Grubb [70], Bozzola and Russell [9].

4.1 Cellulose Nanocrystals

Preparation conditions like hydrolysis time and temperature have great affect on the geometrical properties of resulting CNXLs. Meanwhile, properties such as their diameter, aspect ratio and tendency to aggregate, have critical affects on the mechanical properties of CNXL-polymer composites. Hence, it is important to examine these fillers before they are dispersed in polymer matrices. Various microscopy techniques can be used for this purpose. Most commons are:

Scanning Electron Microscopy (SEM): SEM with a field emission gun (FESEM) can be used to image CNXLs. Usually a dilute solution of the sample is made, a droplet is put on a substrate and is left to air dry. In order to prevent charging and burning either low accelerating voltage (1–3 V) can be used, which

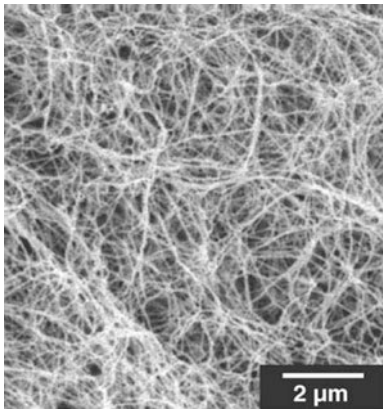

Fig. 23 A SEM image of bacterial CNXL pellicles [59]

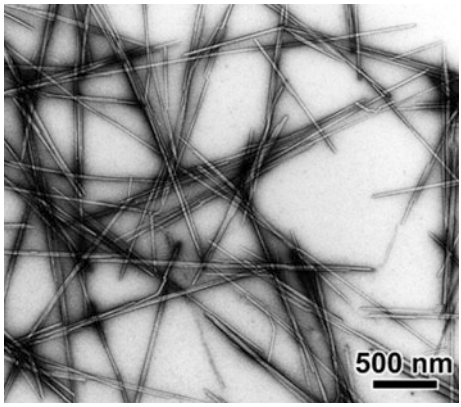

Fig. 24 A TEM image of tunicin CNXL [22]

will degrade the resolution, or the sample can be coated with conducting materials. Because of resolution limitations and instability of the sample in SEMs, it is usually difficult to obtain precise details of CNXLs in these images (Fig. 23).

Transmission Electron Microscopy (TEM): In order to examine CNXLs in TEM, a drop of dilute solution is put on a carbon coated grid, and let dry in air. Usually metal shadowing or negative staining is needed to improve the contrast (Fig. 24). For instance, sample can be negatively stained by floating the grid in staining materials, such as uranyl acetate, for a few minutes. Some difficulties in TEM imaging are sample preparation techniques and beam sensitivity of the sample.

Atomic Force Microscopy (AFM): AFM in tapping mode can be used for this purpose. Again, a droplet of CNXL solution is dried on a substrate (usually freshly cleaved mica) and studied. AFM seems to be a good alternative to electron microscopy because it does not have the limitations of low contrast and resolution, and sample preparation is much easier (Fig. 25). The only disadvantages are the tip broadening and scan rate that can affect the quality of the images.

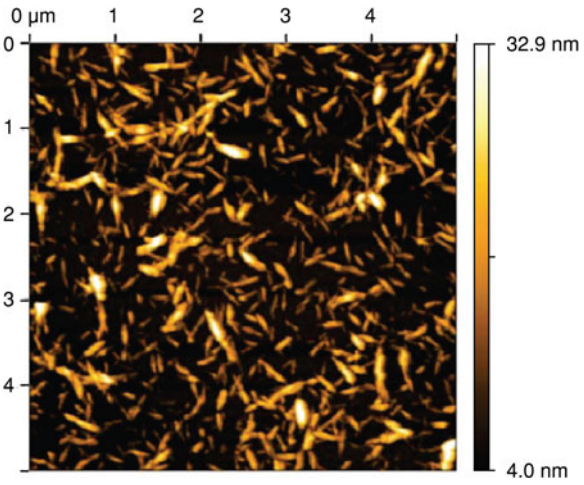

Fig. 25 AFM image of cotton CNXL [22]

4.2 CNXL Polymer Composites

The dispersion quality of CNXL through the polymer matrix has great effects on the nanocomposite ultimate properties. As mentioned before, hydrogen bonding is the main reason for formation of the rigid 3D network of cellulose crystals above percolating threshold, which holds the polymer matrix and improves its mechanical and thermal properties. Meanwhile, these bonds can bring difficulties in filler dispersion, cause aggregation of CNXLs, and degrade the ultimate properties.

Firstly, since the size of CNXLs is smaller than the light wavelength, if the pure polymer is transparent and the final composite comes out opaque, one can conclude that there are agglomerations of CNXLs, simply by eye observations.

Some of the techniques used for characterization of the filler dispersion in nanocomposite materials are: optical microscopy (OM), SEM, TEM, AFM, small angle X-ray scattering (SAXS) and wide angle X-ray diffraction (WAXD). Here we discuss three most common techniques (OM, SEM, TEM). SEM uses electrons to scan the surface of the specimen, and TEM passes electrons through a thin slice of the specimen.

4.2.1 Optical Microscopy

Observation of the solid surface of polymer nanocomposites in an optical microscope (OM) can results in some qualitative information about the filler dispersion. If CNXLs are not individualized and dispersed well, their aggregate will appear in the image (Fig. 26).

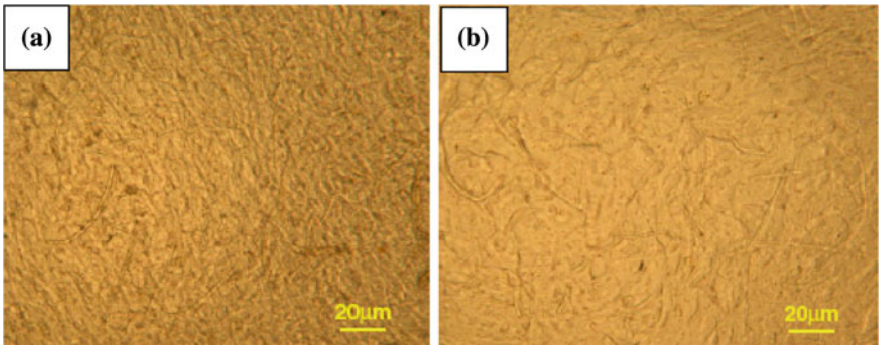

Fig. 26 Optical Microscopy images of CNXL-PVA composites (**a**) reinforcement without coating; (**b**) reinforcement coated with ethylene–acrylic oligomer. The dispersion is better in **b**, where less aggregates and filler with smaller diameters are observed [80]

4.2.2 Scanning Electron Microscopy

The fracture surface of polymer composites (obtained either by cryo fracturing in liquid nitrogen temperature or from tension tests), are observed in SEM and compared to the surface of pure polymer. Addition of CNXLs to polymers alters their fracture mechanism. The fracture surface of thermoplastics is usually featureless, flat and smooth (Figs. 27a, 28a). After CNXLs are added, up till the optimum point, rigid CNXLs act as obstacles for movement of dislocations and cracks and make them change path. As a result the fracture surface comes out to be rough and irregular with coarse slip planes (Figs. 27b, 28b). After this point, addition of more CNXL, results in their agglomeration and inferior mechanical properties and this coincides with voids, wrinkles and crystals being pulled out of the polymer matrix (Fig. 27c).

Usually CNXLs appear as white dots during the SEM imaging due to the highly non-conductive nature of the nanocrystals. The concentration of these dots increases as the filler content increases in the nanocomposite. When CNXLs are well dispersed and there is good adhesion between the filler and the polymer

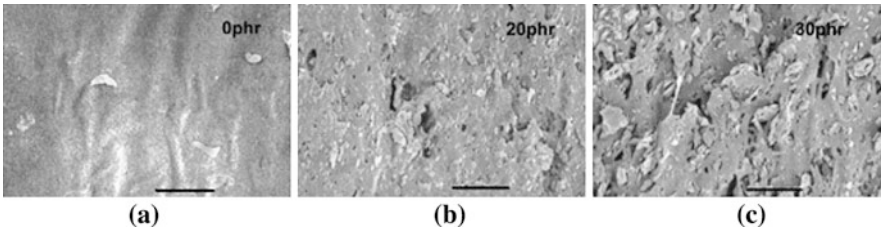

Fig. 27 SEM images of tension fracture surfaces of CNXL/nitrile rubber composites: **a** 0 phr; **b** 20 phr (optimum filler content); **c** 30 phr (The scale bars are 50 microns). Comparing to (**a**), the surface is rougher in (**b**) and (**c**). Because of poor matrix/filler interactions, pulled out particles can be seen in (**c**) [48]

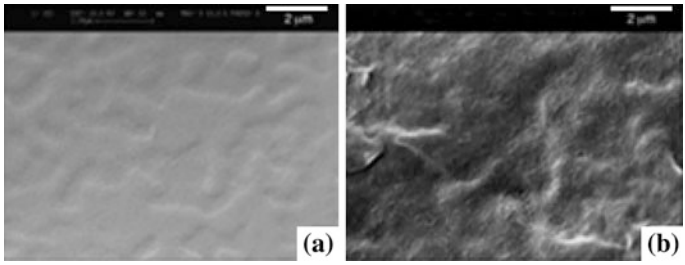

Fig. 28 Fracture surface of polyurethane (**a**) and polyurethane filled with 1 wt. % CNXLs (**b**). CNXLs make the cracks change path and increase the energy dissipation during the fracture in (**b**) [3]

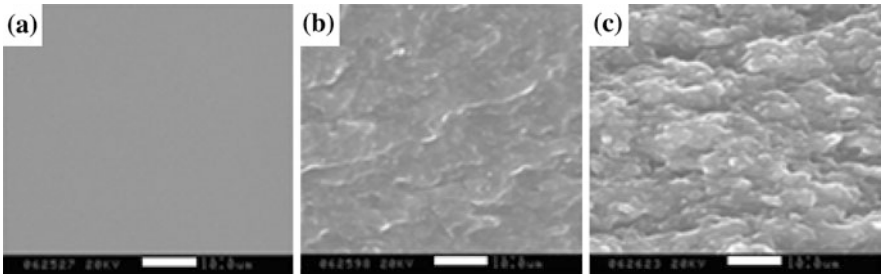

Fig. 29 SEM images of the polyurethane filled with different wt. % of CNXL: **a** 0 **b** 20 **c** 30. In contrast with the fracture surface in (**a**) which is featureless, the fracture surfaces are rough in (**b**) and (**c**) and the white dots on them are the CNXLs [13]

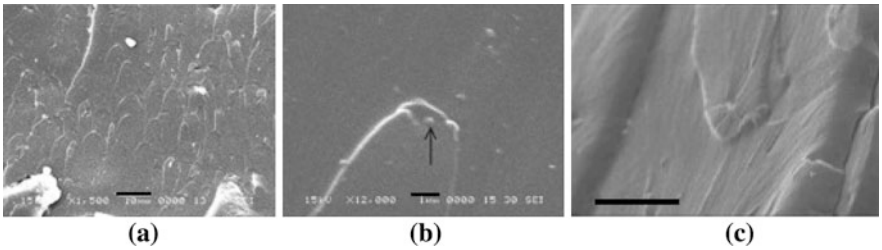

Fig. 30 SEM images of the fish scale feature on the fracture surface of cellulose nanocomposites which is related to the fracture toughness: **a** ×1,500 (scale bar = 10 micron) **b** ×12,000, the *arrow* shows a CNXL (scale bar = 1 micron) **c** the surface from an angle (scale bar = 2 micron) [54]

matrix (e.g. when both phases are hydrophilic) fractography of the fracture surface reveals no sign of agglomeration of nanocrystals (Fig. 29).

Marcovich et al. [54] detected a fish scale feature on the fracture surface of nanocomposites of polyurethane and CNXLs (Fig. 30). The density of these parabolic features is related to the energy consumed to break the samples and thus the

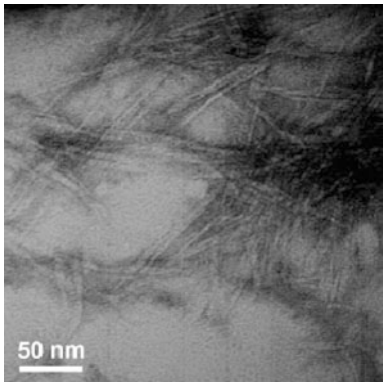

Fig. 31 TEM images of CNXL-PLA composite [47]

fracture toughness. As the content of the filler increases the ridges on the fracture surface become smaller and their density increases. This might results in higher density of crack deflections, and as a consequence higher fracture toughness.

4.2.3 Transmission Electron Microscopy

In this case, very thin (<100 nm) slices of the specimen are prepared using ultra microtome with a diamond knife. These slices are then mounted on carbon coated grids and studied in TEM (Fig. 31). Because the filler and the matrix are both polymers, CNXLs need to be stained (usually negatively, using materials such as uranyl acetate) to improve the contrast. Because of difficulties with respect to sample preparation and also cost, TEM is not used as widely as SEM is.

5 Summary

A limited number of theoretical modeling on mechanics of individual cellulose nanocrystals and their nanocomposites has been conducted so far. There are still great opportunities for computational mechanic researchers to explore this field. First principle calculations and molecular mechanics have the potential to better describe the behavior of cellulose nanocrystals due to their nanometer sizes. Rarely, direct experimental methods have been utilized for measuring the mechanical properties of individual cellulose nanocrystals. An indirect method based on the shift in Raman band peak has been used to obtain the elastic modulus of cellulose nanocrystals embedded in a polymer matrix. These measurments are not reliable due to the effect of background matrix. Recently AFM technique was used to perform bending tests on CNXLs, but this technique has to be further explored.

It has been shown that there is a clear difference in the mechanical properties of CNXLs from different resources. For instance, CNXLs from cotton have smaller aspect ratios and as a result smaller elastic modulus than those from bacteria or tunicate. However no micro/nanoscale observation has been made to understand the atomistic nature of such differences.

The macroscopic mechanical behavior of cellulose nanocomposites can be strongly affected by the competition between filler/filler and matrix/filler interactions and by the formation of strong 3D network of CNXLs. It has been shown that tensile modulus, yield strength, fracture toughness and creep resistance are higher in cellulose nanocomposites than in the neat polymers, but due to the agglomeration of CNXLs in higher filler contents, there is usually an optimum amount of filler. In order for the mechanical percolation to happen filler/filler interactions need to be predominant. On the other hand optimized matrix/filler interactions in nanocomposites guarantees superior mechanical and thermomechanical properties.

Addition of CNXL to polymers also alters their failure mechanism. The fracture surface changes from being smooth and featureless to being rough. As the content of the cellulose increases, there is more discontinuity and stress concentration, and the ridges on the surface of the fracture become denser and smaller. It is expected that the presence of the nanocrystals causes crack deflection during the fracture, and a greater energy is needed for the cracks to grow.

Furthermore, CNXLs improve thermal stability of polymer composites. Formation of rigid 3D CNXL network, which keeps the polymer chains from moving, causes increase in the storage modulus (E', G') and T_g, broadens tan δ peak and moves it to higher temperatures.

Acknowledgments The authors would like to thank Michigan Technological University for providing the financial support to conduct this review.

References

1. Alemdar, A., Sain, M.: Biocomposites, from wheat straw nanofibers: morphology, thermal and mechanical properties. Compos. Sci. Technol. **68**, 557–565 (2007)
2. Angles, M.N., Dufrense, A.: Plasticized starch/tunicin whisker nanocomposite materials 2: mechanical behavior. Macromolecules **34**, 2921–2931 (2001)
3. Auad, M.L., Contos, V.S., Nutt, S., et al.: Characterization of nanocellulose reinforced shape memory polyurethanes. Polym. Int. **57**, 651–659 (2008)
4. Azizi Samir, M., Alloin, F., Dufresne, A.: Review of recent research into cellulosic whiskers, their properties and their applications in nanocomposite field. Biomacromolecules **6**, 612–626 (2005)
5. Azizi Samir, M., Alloin, F., Sanchez, J., et al.: Cellulose nanocrystals reinforced poly(oxyethylene). Polymer **45**, 4149–4157 (2004a)
6. Azizi Samir, M., Alloin, F., Sanchez, J., et al.: Preparation of cellulose whiskers reinforced nanocomposites from an organic medium suspension. Macromolecules **37**, 1386–1393 (2004b)

7. Bondeson, D., Mathew, A., Oksman, K.: Optimization of the isolation of nanocrystals from microcrystalline cellulose by acid hydrolysis. Cellulose **13**, 171–180 (2006)
8. Bodenson, D., Oksman, K.: Dispersion and characterization of surfactant modified cellulose whiskers nanocomposites. Compos. Interfaces **14**, 617–630 (2007)
9. Bozzola, J.J., Russell, L.D.: Electron microcopy: principles and techniques for biologists. Jones and Bartlett Publishers, Boston (1992)
10. Beck-Candanedo, S., Roman, M., Gray, D.G.: Effect of reaction conditions on the properties and behavior of wood cellulose nanocrystal suspensions. Biomacromolecules **6**, 1048–1054 (2005)
11. Beecher, J.: Wood, trees and nanotechnology. Nat. Nanotechnol. **2**, 1–2 (2007)
12. Brown, E.E., Laborie, M.G.: Bioengineering bacterial cellulose/poly (ethylene oxide) nanocomposites. Biomacromolecules **8**, 3074–3081 (2007)
13. Cao, X., Dong, H., Li, C.M.: New nanocomposite materials reinforced with flax cellulose nanocrystals in waterborne polyurethane. Biomacromolecules **8**, 899–904 (2007)
14. Carotenuto, G.C., Her, Y.S., Matijevic, E.: Preparation and characterization of nanocomposite thin films for optical devices. Ind. Eng. Chem. Res. **35**, 2929–2932 (1996)
15. Cheng, Q., Wang, S.: A method for testing the elastic modulus of single cellulose fibrils via atomic force microscopy. Composites **39**, 1838–1843 (2008)
16. Choi, Y., Simonsen, J.: Cellulose nanocrystal-filled carboxymethyle cellulose nanocomposites. J. Nanosci. Nanotechnol. **6**, 633–639 (2006)
17. Daniel, I.M., Ishai, O.: Engineering mechanics of composite materials. Oxford University Press, New York (1994)
18. Dufresne, A., Cavaille, J., Helbert, W.: Thermoplastic nanocomposites filled with wheat straw cellulose whiskers. Part 2. Effect of processing and modeling. Polym. Compos. **18**, 198–210 (1997)
19. Dufresne, A., Dupeyre, D., Vignon, M.R.: Cellulose microfibrils from potato tuber cells: processing and characterization of starch-cellulose microfibril composites. J. Appl. Polym. Sci. **76**, 2080–2092 (2000)
20. Eichhorn, S.J., Sirichaisit, J., Young, R.J.: Deformation mechanisms in cellulose fibers, paper and wood. J. Mat. Sci. **36**, 3129–3135 (2001a)
21. Eichhorn, S.J., Young, R.J., Yeh, W.Y.: Deformation processes in regenerated cellulose fibers. Text. Res. J. **71**, 121–129 (2001b)
22. Elazzouzi-Hafraoui, S., Nishiyama, Y., Pataux, J., Heux, L., Dubreuil, F., Rochas, C.: The shape and size distribution on crystalline nanoparticles prepared by acid hydrolysis of native cellulose. Biomacromolecules **9**, 57–65 (2008)
23. Favier, V., Chanzy, H., Cavaille, J.Y.: Polymer nanocomposites reinforced by cellulose whiskers. Macromolecules **28**, 6365–6367 (1995)
24. Favier, V., Ganova, G.R., Shrivastava, S.C., Cavaille, J.Y.: Mechanical percolation in cellulose whisker nanocomposites. Poly. Eng. Sci. **37**, 1732–1739 (1997)
25. George, J., Sreekala, M.S., Thomas, S.: A review on interface modification and characterization of natural fiber reinforced plastic composites. Poly. Eng. Sci. **41**, 1471–1485 (2001)
26. Giannelis, E.P.: Polymer-layered silicate nanocomposites. Adv. Mater. **8**, 29–35 (1996)
27. Glasser, W.G.: Prospects for future applications of cellulose acetate. Macromol. Symp. **208**, 371–394 (2004)
28. Gopalan Nair, K., Dufresne, A., Gandini, A., Belgacem, M.N.: Crab shell chitin whiskers reinforced natural rubber nanocomposites 3.Effect of chemical modofocation of chitin whiskers. Biomacromolecules **4**, 1832–1835 (2003)
29. Grunert, M., Winter, W.T.: Nanocomposites of cellulose acetate butyrate reinforced with cellulose nanocrystals. J. Polym. Environ. **10**, 27–30 (2002)
30. Guhados, G., Wan, W., Hutter, J.L.: Measurement of single bacterial cellulose fibers using atomic force microscopy. Langmuir **21**, 6642–6646 (2005)
31. Habibi, Y., Dufresne, A.: Highly filled bionanocomposites from functionalized polysaccharide nanocrystals. Biomacromolecules **9**, 1974–1980 (2008)

32. Hajji, P., Cavaille, J.Y., Favier, V., Gauthier, C., Vigier, G.: Tensile behavior of nanocomposites from latex and cellulose whiskers. Polym. Compos. **17**, 612–619 (1996)
33. Hamad, W.: On the development and applications of cellulosic nanofibrillar and nanocrystalline materials.Can. J. Chem. Eng. **84**, 513–519 (2006)
34. Harris, B.: Engineering composite materials. IOM Communications Ltd., London (1999)
35. Helbert, W., Cavaille, J.Y., Dufresne, A.: Thermoplastic nanocomposites filled with wheat straw cellulose whiskers. Part I: processing and mechanical behavior Polym. Compos. **17**, 604–611 (1996)
36. Heux, L., Chauve, G., Bonnini, C.: Nanoflocculating and chiral-nematic self-ordering of cellulose microcrystals suspensions in nonpolar solvents. Langmuir **16**, 8210–8212 (2000)
37. Hongmei, W., Chen, Z., Fang, P., et al.: Synthesis, characterization and optical properties of hybridized CdS-PVA nanocomposites. Mater. Chem. Phys. **106**, 443–446 (2007)
38. Hsieh, Y.C., Yano, H., Nogi, M., et al.: An estimation of the Young's modulus of bacterial cellulose filaments. Cellulose **15**, 507–513 (2008)
39. Hubbe, M.A., Rojas, O.J., Lucia, L.A., Sain, M.: Cellulose nanocomposites: a review. Bioresources **3**, 925–980 (2008)
40. Iwamoto, S., Kai, W., Isogai, A., Iwata, T.: Elastic modulus of single cellulose microfibrils from tunicate measured by atomic force microscopy. Biomacromolecules **10**, 2571–2576 (2009)
41. Kojima, Y., Usuki, A., Kawasumi, M., et al.: One-pot synthesis of nylon-6 clay hybrid. J. Polym. Sci. Part A Polym. Chem. **31**, 1755–1758 (1993)
42. Kojimia, Y., Usuki, A., Okada, A.: J. Polym. Sci. Part A Polym. Chem. **35**, 2289 (1997)
43. Kong, K., Eichhorn, S.J.: The influence of hydrogen bonding on the deformation micromechanics of cellulose fibers. J. Macromol. Sci. B Phys. **44**, 1123–1136 (2005)
44. Koo, C.M., Kim, M.J., Choi, M.H., et al.: Mechanical and rheological properties of the maleated polypropylene-layered silicate nanocomposites with different morphology. J. Appl. Polym. Sci. **88**, 1526–1535 (2003)
45. Kroon, L.M.J., Kroon, L., Northolt, M.G.: Chain modulus and intramolecular hydrogen bonding in native and regenerated cellulose fibers. Polym. Commun. **27**, 290–292 (1986)
46. Kvien, I., Sugiyama, J., Votrubec, M., et al.: Characterization of starch based nanocomposites. J. Mater. Sci. **42**, 8163–8171 (2007)
47. Kvien, I., Tanem, B.S., Oksman, K.: Characterization of cellulose whiskers and their nanocomposites by atomic force and electron microscopy. Biomacromolecules **6**, 3160–3165 (2005)
48. Lapa, V.L.C., Suarez, J.C.M., Visconte, L.L.Y., et al.: Fracture behavior of nitrile rubber-cellulose II nanocomposites. J. Mater. Sci.**42**, 9934–9939 (2007)
49. Lee, S., Wang, S., Pharr, G.M., et al.: Evaluation of interphase properties in a cellulose fiber reinforced polypropylene composites by nanoindentation and finite element analysis. Composites **38**, 1517–1524 (2007)
50. Ljungberg, N., Cavaille, J.Y., Heux, L.: Nanocomposites of isotactic polypropylene reinforced with rod-like cellulose whiskers. Polymer **47**, 6285–6292 (2006)
51. Lyons, W.J.: Theoretical value of the dynamic stretch modulus of cellulose. J. Appl. Phys. **30**, 796–797 (1959)
52. Lu, Y., Weng, L., Cao, X.: Morphological, thermal and mechanical properties of ramie crystallites-reinforced plasticized starch bio composites. Carbohydr. Polym. **63**, 198–204 (2006)
53. Mann, J., Roldan-Gonzalez, L.: X-Ray measurements of the elastic modulus of cellulose crystals. Polymer **3**, 549–553 (1962)
54. Marcovich, N.E., Auad, M.L., Bellesi, N.E., et al.: Cellulose micro/nanocrystals reinforced polyurethane. J. Mater. Res. **21**, 870–881 (2006)
55. Meyer, K.H., Lotmar, W.: Helvetica Chem. Acta. **19**, 68 (1936).
56. Mi, Y., Zhang, X., Zhou, S., et al.: Morphological and mechanical properties of bile salt modified multi-walled carbon nanotube/poly(vinyl alcohol) nanocomposites. Compos. Part A Appl. Sci. Manuf. **38**(n9), 2041–2046 (2007)

57. Mohanty, A.K., Misra, M., Drzal, L.T.: Surface modifications of natural fibers and performance of the resulting biocomposites: an overview. Compos. Interfaces **8**, 313–343 (2001)
58. Muller, F.A., Muller, L., Hofmann, I., et al.: Cellulose-based scaffold materials for cartilage tissue engineering. Biomaterials **27**, 3955–3963 (2006)
59. Nakagaito, A.N., Iwamoto, S., Yano, H.: Bacterial cellulose: the ultimate nano-scalar cellulose morphology for production of high strength composites. Appl. Phys. **80**, 93–97 (2005)
60. Nishino, T., Takano, K., Nakamae, K.: Elastic modulus of the crystalline regions of cellulose polymorphs. J. Polym. Sci. B Polym. Phys. **33**, 1647–1651 (1995)
61. Noorani, S., Simonsen, J., Atre, S.: Nanoenabled microtechnology: Polysulsone nanocomposites incorporating cellulose nanocrystals. Cellulose **14,** 577–584 (2007)
62. Oliver, W.C., Pharr, G.M.: An improved technique for determining hardness and elastic modulus using load and displacement sending indentation experiments. J. Mater. Res. **7**, 1564–1583 (1992)
63. Orts, W.J., Shey, J., Imam, S.H., Glenn, G.M.: Guttman M E, Revol J, Application of cellulose microfibrils on polymer nanocomposites. J. Polym. Environ. **13**, 301–306 (2005)
64. Peng, Z., Xue, L.X., Li, S.D.: Dynamic mechanical analysis of polyvinylalcohol/silica nanocomposite. Synth. Met. **152**(n1–3), 25–28 (2005)
65. Petersoon, L., Kvien, I., Oksman, K.: Structure and thermal properties of poly(lactic acid)/ cellulose whiskers nanocomposite materials. Compos. Sci. Tech. **67**, 2535–2544 (2007)
66. Roman, M., Winter, W.T.: Cellulose nanocrystals. From discovery to application TAPPI international conference on nanotechnology, Atlanta. Georgia (2006)
67. Roohani, M., Habibi, Y., Belgasem, N.M., Ebahim G.: Cellulose whiskers reinforced polyvinyl alcohol copolymers nanocomposites. Eur. Polym. J. **44**, 2489–2498 (2008)
68. Rusli, R., Eichhorn, S.J.: Determination of the stiffness of cellulose nanowhiskers and the fiber-matrix interface in a nanocomposite using Raman spectroscopy. Appl. Phys. Lett. **93**, 033111 (2008)
69. Sakurada, I., Nukushina, Y., Ito, T.: Experimental determination of the elastic modulus of the crystalline regions in oriented polymers. J. Polym. Sci. **57**, 651–660 (1962)
70. Sawyer, L.C., Grubb, D.T.: Polymer microcopy 2nd edition. Chapman and Hall, London, New York (1996)
71. Schmidt, H., Krug, H., Kasemann, R., et al.: Development of optical waveguides by sol-gel techniques for laser patterning. Proc. SPIE Int. Soc. Opt. Eng. **1590**, 36–43 (1991)
72. Shibata, M., Oyamada, S., Kobayashi, S., et al.: Mechanical composites and biodegragability of green composites based on biodegradable polyesters and lyocell fabric. J. Appl. Polym. Sci. **92**, 3857–3863 (2004)
73. Sturcova, A., Davies, G.R., Eichhorn, S.J.: Elastic modulus and stress-transfer properties of tunicate cellulose whiskers. Biomacromolecules **6**, 1055–1061 (2005)
74. Tanaka, F., Iwata, T.: Estimation of the elastic modulus of cellulose crystal by molecular mechanics simulation. Cellulose **13**, 509–517 (2006)
75. Tashiro, K., Kobayashi, M.: Theoretical evaluation of three-dimensional elastic constants of native and regenerated cellulose: role of hydrogen bonds. Polymer **32**, 1516–1526 (1991)
76. Tranchida, D., Piccarolo, S., Loos, J., Alexeev, A.: Mechanical characterization of polymers on nanometer scale through nanoindentation. A study on pile-up and viscoelasticity. Macromolecules **40**, 1259–1267 (2007)
77. Treloar, L.R.G.: Calculation of elastic moduli of polymer crystals: III. Cellulose Polym. **1**, 290–303 (1960)
78. Vaia, R.A., Ishii, H., Giannelis, E.P.: Synthesis and properties of 2D nanostructures by direct intercalation of polymer melts in layered silicates. Chem. Mater. **5**, 1694–1696 (1996)
79. Wang, Y., Cao, X., Zhang, L.: Effect of cellulose whiskers on properties of soy protein thermoplastics. Macromol. Biosci. **6**, 524–531 (2006)
80. Wang, B., Sain, M.: Isolation of nanofibers from soybean source and their reinforcing capability on synthetic polymers. Compos. Sci. Tech. **67**, 2521–2527 (2007)

81. Wung, C.J., Yang, Y., Prasat, P.N., et al.: Poly(p-phenylene vinylene)-silica composite. A novel sol-gel processed non-linear optical material for optical waveguides. Polymer **32**, 605–608 (1991)
82. Yongshang, L., Weng, L., Cao, X.: Morphological, thermal and mechanical properties of ramie crystallites-reinforced plasticized starch biocomposites, Carbohyd. Polym. **63**, 198–204 (2005)
83. Yu, M.F., Lourie, O., Dyer, M.J., et al.: Strength and breaking mechanism of multi walled carbon nanotubes under tensile load. Science **287**, 637–640 (2000)
84. Zimmermann, T., Pohler, E., Schwaller, P.: Mechanical and morphological properties of cellulose fibril reinforced nanocomposites. Adv. Eng. Mater. **7**, 1156–1161 (2005)
85. Zugenmaier, P.: Conformation and packing of various crystalline cellulose fibers. Prog. Polym. Sci. **26**, 1341–1417 (2001)